The kinetics of cellular patterns

1992 J. Phys.: Condens. Matter 4 1867

(http://iopscience.iop.org/0953-8984/4/8/004)

J. Phys.: Condens. Matter 4 (1992) 1867–1894. Printed in the UK

REVIEW ARTICLE

The kinetics of cellular patterns

James A Glazier†§ and Denis Weaire‡
† Tohoku University, Research Institute of Electrical Communication, Sendai 980, Japan
‡ Trinity College, Dublin, Department of Physics, Dublin 2, Ireland

Received 12 November 1991

Abstract. Many materials, including soap froths, polycrystalline alloys, ceramics, lipid monolayers and garnet films, have structures composed of either two- or three-dimensional polygonal domains separated by well defined boundaries. Usually, the surface energy of these boundaries makes the pattern unstable, causing certain grains to shrink and eventually to disappear. Thus the pattern coarsens continuously unless other factors arrest the motion of the boundaries. We review recent theoretical, computational and experimental progress in our understanding of the asymptotic scaling laws that describe coarsening. In most cases the elementary expectation, that the mean grain radius scales with the square root of time, is confirmed. We pay particular attention to the history of the field, to understand why this elementary result has remained in doubt until now.

1. Introduction

Many naturally occurring structures, from the common soap froth to the large-scale distribution of galaxies in the universe (if we are to believe recent cosmological theories (Lindly 1991)), consist of statistically homogeneous domains separated from each other by distinct boundaries (see table 1). These boundaries are associated with an interfacial energy (surface energy in three dimensions, wall energy in two dimensions). If the total energy is simply the product of the boundary area times a 'surface tension' or surface energy, any reduction in total interfacial area will reduce the energy. Hence such structures are intrinsically unstable, always evolving towards patterns with less surface area, unless other factors (such as boundary pinning or short-range repulsive forces) intervene. The basic mechanism to reduce interfacial area is the elimination of entire domains. Hence the structure coarsens. In the simplest cases, the coarsening is without limit, other than that imposed by the finite size of the system.

One may therefore ask the question: what asymptotic scaling law governs this type of growth? This question has been investigated in a variety of contexts for the past 50 years or more, but there has been particularly rapid progress during the past five years. In this review we will summarize our current state of understanding, and discuss the history of the many misconceptions and misinterpretations that have occurred.

We will focus primarily on the evolution of two-dimensional rather than three-dimensional cellular patterns because the experiments and theory are more tractable and therefore better understood. On the experimental side, this results from the difficulty

§ Permanent address: Department of Physics, University of Notre Dame, Notre Dame, IN 46556, USA.

0953-8984/92/081867 + 28 $04.50

Table 1. Froths and their designations.

System	Designation	Reference
Soap froth	Bubbles	Glazier (1989)
Lipids	Bubbles	Berge *et al* (1990)
Metal	Grains	Atkinson (1988)
Ceramics	Grains	Brook (1976)
Potts model	Domains	Glazier *et al* (1990)
Iron garnets	Domains	Weaire *et al* (1991)
Cucumber	Cells	Lewis (1923)
Cornea of eye	Cells	McDermott *et al* (1990)
Geography	Teritories	Gettis and Boots (1978)
Universe	Voids	Lindly (1991)

of serial sectioning and three-dimensional reconstruction in the direct 'brute force' approach to structural analysis. While light scattering techniques offer more expedient methods of measurement, they can provide only incomplete information about the structure of a froth. On the theoretical side, the computations are much more cumbersome in three dimensions, and the elegant mean-field theories that are made possible by the existence in two dimensions of a local topological rule for the rate of growth or shrinkage of individual bubbles (von Neumann's law (von Neumann 1952)) are not available.

Because of the many fields in which cellular patterns occur, the terminology is somewhat confusing, as table 1 indicates. We shall usually refer to the domains as bubbles or grains.

We will focus on soap froths because of Smith's original insight (Smith 1952, 1954, 1964a, b) that the soap froth represents the closest approach in an experimental system to ideal grain growth. Bragg and Nye (1947) had proposed even earlier that soap froths could be used to model grain growth in metals, but had not realized that the individual bubbles may in some circumstances be regarded as corresponding not to atoms in a crystalline lattice but to entire crystal grains.

We will largely restrict our attention to scaling exponents. For additional information, refer to the many reviews and specialized papers on grain growth. General reviews include Abbruzzese (1992), Glazier (1989), Atkinson (1988) and Weaire and Rivier (1984).

2. Two-dimensional cellular patterns

A cellular pattern is a two-dimensional network of boundary lines meeting (usually) in threefold vertices. We consider cases where the dynamics are driven by surface tension (or surface energy) forces. The topology and dynamics are related since the dominance of threefold vertices results from their structural stability. Fourfold vertices split into pairs of threefold vertices to reduce the boundary length, as shown in figure 1 (Gardner 1986). Secondary effects such as the presence of Plateau borders (section 15) can stabilize fourfold vertices (Bolton and Weaire 1991, 1992). The domains outlined by these boundaries are generally approximately polygonal in shape (though magnetic bubbles

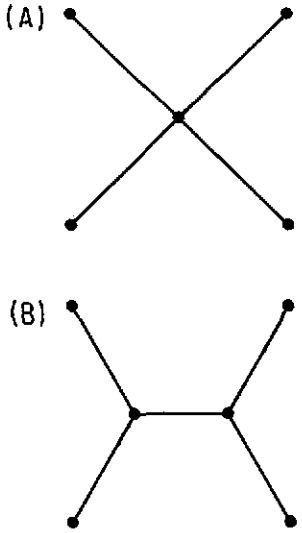

Figure 1. Instability of a fourfold vertex: (A) four points connected to a single fourfold vertex (total length 2.828) decay into (B) four points connected to two threefold vertices (total length 2.732). Since surface tension tends to minimize side length, (A) dissociates into (B).

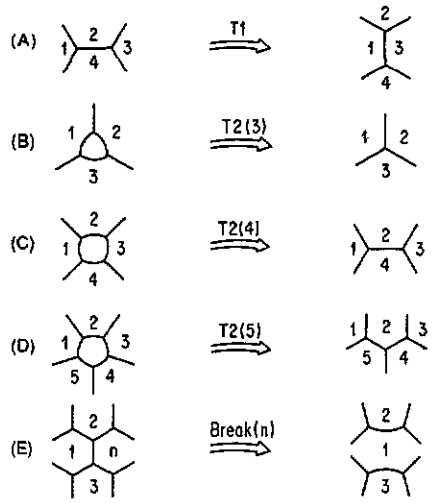

Figure 2. Elementary topological processes in two dimensions. (A) T1 process—side swapping. (B) T2(3) process—disappearance of a three-sided bubble. (C) T2(4) process—disappearance of a four-sided bubble. (D) T2(5) process—disappearance of a five-sided bubble. (E) Wall breakage next to an *n*-sided bubble. Numbers are keyed to column headings in table 2.

present an extreme case where this observation fails), with more or less uniformly curved boundaries.

In ideal soap froths, magnetic bubbles and lipid monolayers, the equilibration time of the boundaries is short compared to the rate at which bubbles grow or shrink, so the pattern is relaxed, or equilibrated. In metal grains, the rates of diffusion along and across grain boundaries are comparable. In the first case we find minimal surfaces of constant total curvature and internal angles at vertices of 120° (Plateau 1843, 1873). In the latter case, both the curvature and vertex angles can vary because of the failure to reach equilibrium and because of the effects of anisotropy.

Similar geometrical rules hold in three dimensions, but vertices are fourfold with 109.47° internal angles. The mean curvature of each bubble wall must be uniform at all points (since the pressure within each bubble is uniform), so the wall can assume the shape of an arbitrary minimal surface (Almgren and Taylor 1976). Some of the geometrical rules that simplify consideration of two-dimensional networks are lost in three dimensions, considerably complicating the problem (Avron and Levine 1992).

3. Topological processes

In the soap froth in two dimensions there are two basic types of topological transformation (see figure 2 and table 2). As shown in figure 2(A), two bubbles can push together and push apart two other bubbles. This is called a T1 process or side swapping.

Table 2. Topological transformations. Keyed to figure 2. The column numbers refer to the bubble numbers for the corresponding topological process in the figure.

Change process	Bubble index				
	1	2	3	4	5
T1	+1	−1	+1	−1	—
T2(3)	−1	−1	−1	—	—
T2(4)	−1	0	−1	0	—
T2(5)	−1	+1	−1	0	0
Break (n)	$+n-4$	−1	−1	—	—

The second basic process is bubble disappearance or the T2 process. In the soap froth, three-sided (T2(3)), four-sided (T2(4)) and five-sided (T2(5)) bubbles can disappear as shown in figures 2(B–D). Additional topological transformations, for example wall breakage in froths (figure 2(E)), grain coalescence in metals or mitosis in cells (the inverse of figure 2(E)), can result in totally different classes of patterns.

The speed of these transformations is much faster than the diffusion-driven area changes and most models assume that they occur instantaneously.

4. Distribution functions

Besides its overall length scale, the two basic characteristics of a given two-dimensional pattern are its area distribution function $\rho(a/\langle a\rangle)$, the probability that a given bubble has a given area a relative to the mean area of the pattern $\langle a\rangle$, and the topological distribution function $\rho(n)$, the probability that a bubble in the pattern has n sides. There are also various area–area, area–topology and topology–topology correlation functions, which we need not consider. In three dimensions, the basic distributions are $\rho(v/\langle v\rangle)$, the probability that a grain has a given volume v relative to the mean volume $\langle v\rangle$, and $\rho(f)$, the probability that a given grain has f faces. There are additional distribution and correlation functions since the number of faces does not uniquely determine the shape of a polyhedron.

Because of the limited statistics usually available, it is often convenient to characterize the distribution functions by their moments. We define the area moments of the distribution to be

$$\mu_m^{\mathrm{A}} \equiv \int \rho(x)(x-1)^m \,\mathrm{d}x \tag{1}$$

where $x \equiv a/\langle a\rangle$. We define the topological moments of the distribution to be

$$\mu_m \equiv \sum_n \rho(n)(n-\langle n\rangle)^m. \tag{2}$$

Higher-order moments are very sensitive to the large-n/large-a tails of the distributions, where statistics are poor, so only the first few moments are useful.

5. Boundary motion and von Neumann's law

In general, boundary curvature drives boundary motion. The soap froth looks somewhat different from grain growth in a metal since the curvature of a bubble wall is constant while that of a metal grain varies from place to place. Nevertheless, we can regard both cases as different limits of a single model, which we call a viscous froth.

For the soap froth, the rate of transfer of area between bubbles i and j is generally assumed to be proportional to both the pressure difference $p_i - p_j$, and the length of the boundary l_{ij}, between them. The area transfer per unit time is

$$\Delta a_{i\to j} = \kappa(p_i - p_j)l_{ij} \tag{3}$$

where κ is a diffusion constant. In the soap froth, this relation is essentially Fick's law.

Neglecting inertia, the balance of forces on a point on a bubble boundary is

$$p_i - p_j = \sigma c - \lambda v_\perp \tag{4}$$

where σ is the surface tension, or surface energy, c is the local curvature of the boundary, λ is the coefficient of viscous drag and $v_\perp$ is the normal velocity of the boundary. This balance of forces is related in an obvious way to the area change of a bubble:

$$\frac{da_i}{dt} = \oint_{\text{bubble } i} v_\perp \, dl. \tag{5}$$

Using equations (3) and (4) we find that

$$\frac{da_i}{dt} = \oint_{\text{bubble } i} c \, dl - \lambda\kappa \frac{da_i}{dt} \tag{6}$$

so that

$$\frac{da_i}{dt} = \frac{\kappa\sigma}{1 + \lambda\kappa} \oint_{\text{bubble } i} c \, dl. \tag{7}$$

Using the definition of curvature, this becomes

$$da_i/dt = [\kappa\sigma/(1 + \lambda\kappa)]\phi \tag{8}$$

where ϕ is the total angle through which the tangent turns on a closed path around the grain, excluding the discontinuous angle changes at the vertices. At each vertex the angle changes by $\pi/3$, and the total angle change is 2π, so

$$\phi = 2\pi - n\pi/3 = (6 - n)\pi/3. \tag{9}$$

Substituting for ϕ yields von Neumann's law (von Neumann 1952):

$$da_i/dt = \kappa'(n - 6) \tag{10}$$

where $\kappa' = \pi\kappa\sigma/[3(1 + \lambda\kappa)]$.

In the limit $\lambda \to 0$ with cell wall curvatures determined by equation (10), we recover the soap froth model of von Neumann's original derivation. In the limit $\lambda \to \infty$ we obtain idealized metallic grain growth, since the pressure differences become negligible and boundary velocities are simply proportional to *local* curvature. In both cases, the rate of increase or decrease of a cell's area depends only on its number of sides. The two limits represent canonical models for soap froth and grain growth, respectively, and

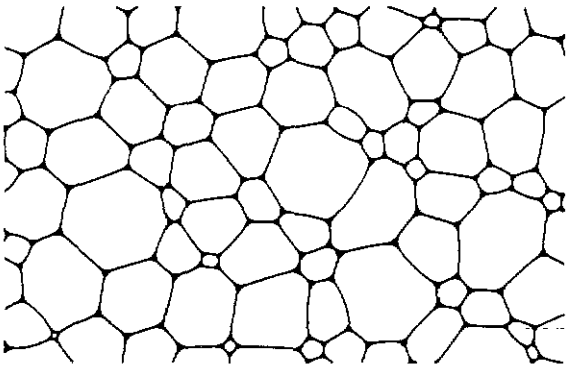

Figure 3. Structure produced by a direct simulation of soap froth with Plateau borders. From Bolton and Weaire (1991).

have both been realized in direct numerical simulations, the former by Weaire and Kermode (1983b) and the latter by Frost *et al* (Frost and Thompson 1986, 1987a, b, Frost *et al* 1988, Howe 1987, Thompson *et al* 1987).

If we had assumed an n-dependent typical internal angle $\theta(n)$, the same derivation would follow to obtain the generalized result for an n-sided cell i (Glazier and Stavans 1989):

$$da_i/dt = \kappa'\{3n[\pi - \theta(n)]/\pi - 6\}. \tag{11}$$

The only pattern that is stable under von Neumann's law is one that has only six-sided cells. Introducing even a single defect pair into a perfect hexagonal lattice results in the collapse and eventual disappearance of all the bubbles in the lattice.

Von Neumann's law is not a complete description of the dynamics of a froth. It describes only the growth of bubbles with fixed numbers of sides. During the evolution of a froth, bubbles typically change their number of sides many times. Whenever a bubble disappears, some of its neighbours change their number of sides (see table 2). Any complete description of the evolution of the soap froth must make additional assumptions about how side redistribution takes place.

The above equation for von Neumann's law with n-dependent vertex angles arose in connection with the study of the effects of *Plateau borders* (PB), the finite liquid accumulations at vertices in a soap froth (see figure 3). In early work they were entirely ignored, so the theory and interpretation of experiments assumed a foam with negligible liquid fraction, a *dry* foam.

In the opposite extreme, the liquid fraction is so high that the bubbles are round and effectively isolated from each other (see figure 23(A)). In this case the rate of diffusion of gas from a bubble depends not only on its wall curvature but on the average pressure generated by all the bubbles in the pattern. This background pressure supplies area to bubbles at the same time as their curvatures cause them to lose area. While the derivation contains some subtleties, the same general argument that leads to von Neumann's law yields:

$$da(r)/dt = \kappa'(B - 1/r) \tag{12}$$

where B is an unknown background pressure term, which is uniform throughout the pattern but which may vary in time. Conservation of the total bubble area then requires

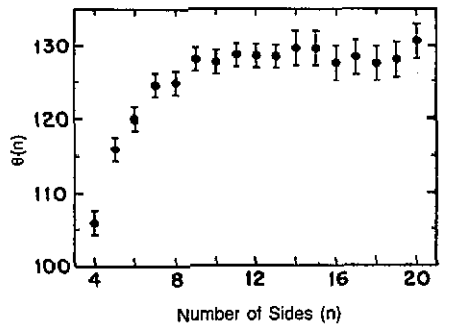

Figure 4. Internal angles in the soap froth. Average internal angles $\theta(n)$ of n-sided bubbles. Error bars show one standard deviation in the measured data. from Stavans and Glazier (1989).

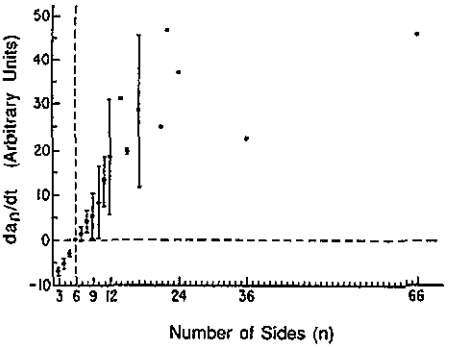

Figure 5. Von Neumann's law. Growth rates for n-sided bubbles. Error bars show one standard deviation in the measurement. Single points indicate that only one measurement was made for that number of sides. From Glazier and Stavans (1989).

that $B = \langle 1/r \rangle$, so that we obtain the Lifschitz–Slyozov rule for the growth of isolated bubbles (Lifschitz and Slyozov 1959, 1961):

$$da(r)/dt = \kappa'(\langle 1/r \rangle - 1/r). \tag{13}$$

In fact, Lifschitz and Slyozov used $B = 1/\langle r \rangle$ so that area was not conserved, but this difference does not greatly affect the result. As in the von Neumann's law case, small bubbles shrink and vanish and large bubbles grow, but the kinetics of the evolution is different and easier to simulate owing to the absence of discontinuous topological transformations.

6. Von Neumann's law: experimental results

Von Neumann's law was first checked experimentally by Glazier *et al* (1987) and Fu (1988). They found that, to within the accuracy of their experiment, von Neumann's law was verified, *on average*, for ensembles of bubbles with up to nine sides, but failed for individual bubbles, e.g. some five-sided bubbles grew and some seven-sided bubbles shrank. However, some of their spread in growth rate may have been due to measurement error. They also found that, within the accuracy of their measurements, the diffusion constant κ' in von Neumann's law remained constant. This posed a problem since the derivation of von Neumann's law is strictly local: it should be obeyed by each bubble individually.

The discrepancy was partly explained by the measurements of Stavans and Glazier (1989), which showed that the average internal angles of bubbles were not exactly 120° (see figure 4). The observed angle deviations had a fairly large spread. The more recent and careful measurement of von Neumann's law by Glazier and Stavans (1989) used a froth in which a few large, many-sided bubbles had been intentionally introduced. Their measurements verified the ensemble form of von Neumann's law for bubbles with up to 30 sides (see figure 5). They also observed a slight deviation from linear behaviour for few-sided bubbles, and showed that this deviation was compatible with the observed angle deviations according to equation (11). Since the angle deviations were statistical

in nature, they proposed that they were the origin of the observed fluctuations in the growth rates of individual bubbles. More recently Weaire and Bolton (1990) have shown that the presence of PB can result in the observed angle and von Neumann's law deviation. Such angle deviations have also been observed by Stine *et al* (1990) in lipid monolayers. Recent work by Stavans (1990) in a drained froth with extremely narrow PB confirms that in a dry froth the angle deviations disappear and that von Neumann's law is obeyed by individual bubbles.

7. Scaling states

A pattern in either two or three dimensions is in a *scaling state* if all of its distribution and correlation functions for all dimensionless quantities are constant in time. In this case the only property of the pattern that can vary is its mean length scale.

Von Neumann's law predicts that, in a scaling state, the average area of a bubble $\langle a \rangle$ is proportional to the time t, i.e. the average length scale goes like t^{β} where $\beta = 0.5$. The simplest argument is dimensional: the pattern is characterized in a scaling state by a single length scale, the mean cell radius $\langle r \rangle$, with units of metres. The mean radius is a function of time, units of seconds, and the only parameter κ' has units of metres squared per second. Thus the only dimensionally correct combination of these three quantities in the form of a power law is

$$\langle r \rangle \propto (\kappa')^{0.5} t^{0.5} \qquad \Rightarrow \qquad \beta = 0.5. \tag{14}$$

The Lifschitz–Slyozov growth law (equation (13)) yields a different growth exponent on dimensional grounds. As before, in a scaling state, the only length scale is the mean radius $\langle r \rangle$, and the only parameter κ' has units of metres cubed per second, so the only dimensionally correct combination of these three quantities in the form of a power law is

$$\langle r \rangle \propto (\kappa')^{0.33} t^{0.33} \qquad \Rightarrow \qquad \beta = 0.33 \tag{15}$$

so the β for Lifschitz–Slyozov growth and von Neumann's law growth are different.

8. Determination of the growth exponent

Surprisingly, since it is the central issue in the analysis, there has been relatively little attention paid to the technique used to determine the growth exponent. Typically the average bubble size is measured a a function of time, plotted on a log–log plot, and the slope is determined by linear regression. This process is subject to several types of error.

The region in time over which the scaling state is achieved is difficult to determine from the area data alone, and thus there is a tendency to include too much short-time data, which generally lowers the measured exponent. Many people seem to accept that a system is in a scaling state whenever it exhibits power-law growth. However, because of the difficulty of measuring growth exponents and distinguishing between power-law and non-power-law growth, this assumption should be avoided. Instead, one should determine the onset of the scaling state independently, e.g. by requiring that $\rho(n)$ and $\rho(a/\langle a \rangle)$ be constant. Practically, we may accept that any pattern in which μ_2 is constant is in a scaling state.

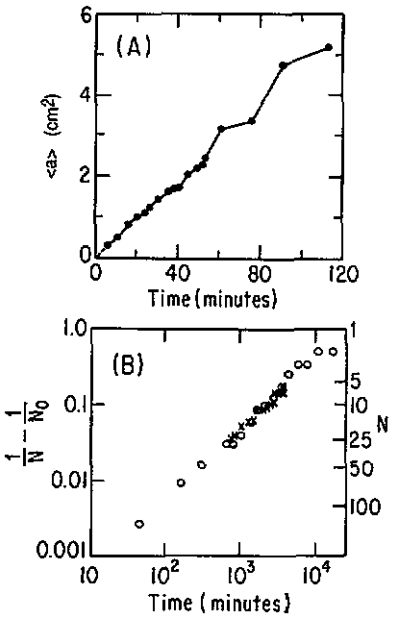

Figure 6. Area growth in soap froth. Early experimental data on area growth in two-dimensional soap froth. (A) Average area versus time. From Smith (1952). (B) Average area (=1/number of bubbles, N) versus time for experiment (○) and vertex model (×). From Fullman (1952).

The range of length scales over which the exponent is measured is rarely as much as a full decade, since the pattern usually must grow by an order of magnitude in area to reach a well behaved scaling state. It is difficult to make the initial length scale sufficiently small that there are many grains left in the scaling state. The result is that the uncertainties in exponent can be very large, and it is difficult to determine unambiguously whether the growth is consistent with a power law. The only remedy is to use the largest possible system, and the smallest possible initial grain size.

Finally, the time origin is essentially arbitrary, and this can affect the fit at short times. This problem is particularly serious when the measurements are made at logarithmic intervals in time, so that shorter times are more heavily represented. It is better to fit directly the expected form of the grain growth,

$$r(t) = (t - t_0)^{\beta} \tag{16}$$

by adjusting t_0 and β.

9. Early history of scaling for the two-dimensional soap froth

In his initial study of soap froths, Smith (1952) found that the areas of soap bubbles in a sealed cell grew linearly in time, $\beta = 0.5$ (figure 6(A)). He used air in a sealed circular glass cell at a pressure close to the vapour pressure of water (to increase the rate of change of area) and applied vigorous shaking to produce an initially disordered froth with a few thousand tiny bubbles, which rapidly evolved to a few hundred bubbles with a bubble diameter of between one and two millimetres. This initial condition corresponded closely to the metallic systems he was trying to model in which growth began from many nucleation sites separated by atomic length scales. At nearly the same

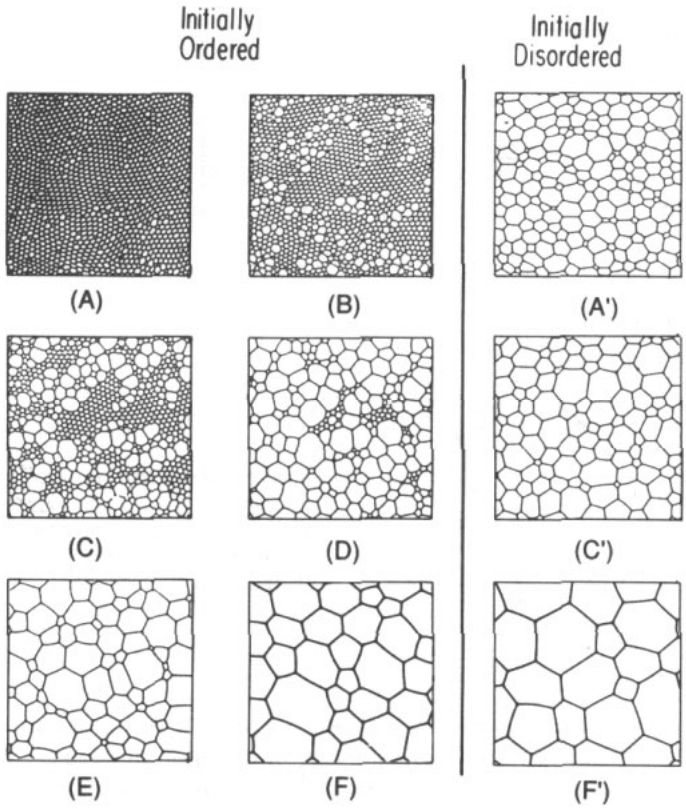

Figure 7. Evolution of a soap froth pattern, for initially ordered (left) and initially disordered (right) states. Times are: (A) 1 h, (B) 2.52 h, (C) 4.82 h, (D) 8.63 h, (E) 19.87 h, (F) 52.33 h; (A') 1.95 h, (C') 21.50 h, (F') 166.15 h. From Glazier *et al* (1987).

time, Fullman (1952) independently obtained the same result (figure 6(B)) in a medium-pressure sealed container.

That should probably have been definitive, except that Smith repeated his experiment with a slightly different method, beginning with bubbles blown individually with fairly uniform size. Aboav, analysing these data, obtained a value of $\beta = 1.0$. He also found that μ_2 grew linearly in time (Aboav 1970). Weaire and Kermode (1983a) suggested that the result might be a fractal soap froth, with bubbles at all length scales (such structures were later studied by Herdtle and Aref (1991a) and shown to be unstable). The development of such a fractal structure from an initially homogeneous length scale would imply that there was no scaling state in the evolution, as in Lifschitz–Slyozov coarsening. This was an intriguing possibility, and excited much new experimental and theoretical effort.

Fu (1988) also studied the evolution of a froth by photographing under a microscope the very small air bubbles in a cell made from microscope slides but was unable to determine a consistent value for β.

Glazier *et al* (1987) repeated Smith's second experiment using a series of large sealed rectangular experimental cells beginning with individual bubbles of a fairly uniform size. They showed that Aboav's high β and increasing μ_2 were due to *transient* effects. An

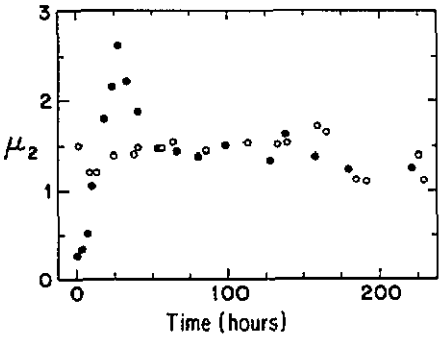

Figure 8. Evolution of μ_2 versus time in the two-dimensional soap froth, for an initially ordered state (●) and an initially disordered state (○). From Stavans and Glazier (1989).

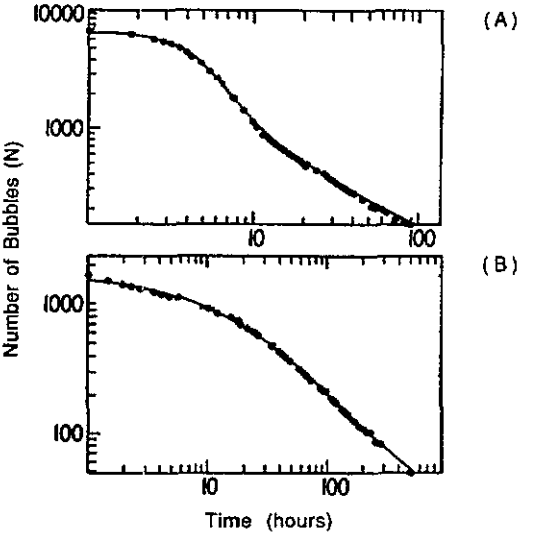

Figure 9. Average number of bubbles ($1/\langle a \rangle$) versus time in the two-dimensional soap froth: (A) for an initially ordered state ($\beta = 0.34 \pm 0.02$) and (B) for an initially disordered state ($\beta = 0.4 \pm 0.04$). From Glazier *et al* (1987).

initial pattern composed of bubbles of fairly uniform size organizes itself into patches of regular hexagons, which do not evolve (see figure 7). Only the bubbles with $n \neq 6$ at the grain boundaries can grow or shrink. Hexagonal patches can only disorder at their boundaries as bubbles change their number of sides owing to the disappearance of neighbouring bubbles. The spread of disorder is diffusive and therefore the rate of evolution is slow. Because these hexagonal patches retain the initial length scale of the pattern, they must disappear before a scaling state can be reached.

At intermediate times there are large evolving bubbles, as well as many small bubbles at the original length scale. The large bubbles have many sides and grow rapidly since they are surrounded by much smaller bubbles. The result is very rapid evolution and an effective $\beta > 0.5$, as noted by Aboav (1970). At the same time the mixture of evolved and original length scales increases β, μ_2 and μ_2^{A}. When the original length scale finally disappears, β, μ_2 and μ_2^{A} decrease to their scaling state values (Stavans and Glazier 1989). The evolution of μ_2 is shown in figure 8. Sometimes there is a second oscillation of μ_2 (Glazier 1989, Glazier *et al* 1990a).

Regardless of initial conditions, all Glazier *et al*'s patterns eventually reached a regime in which the area grew as a power law and $\rho(n)$ was constant (see figure 9). However, they measured a growth exponent of $\beta = 0.34$. An obvious possibility was that κ' in von Neumann's law decreased with time. However, they found it to be constant. They reluctantly concluded that the pattern did not reach a scaling state. Such a conclusion had been suggested by the Potts model simulations of Grest *et al* (1984), which appeared to have $\beta = 0.4$, and by the fractal hypothesis of Weaire and Kermode (1983a). It was also supported by the observation that, in metals, β was usually less than 0.5 (see table 3) (Martin and Doherty 1976).

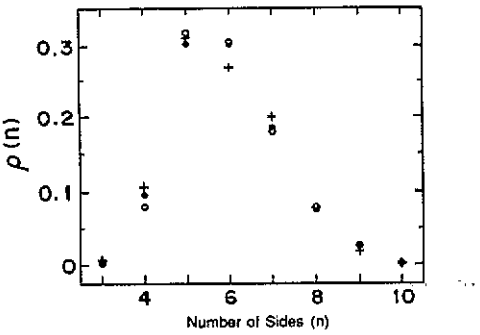

Figure 10. Steady-state topological distribution function $\rho(n)$ for a two-dimensional soap froth in a scaling state at three different times. From Stavans and Glazier (1989).

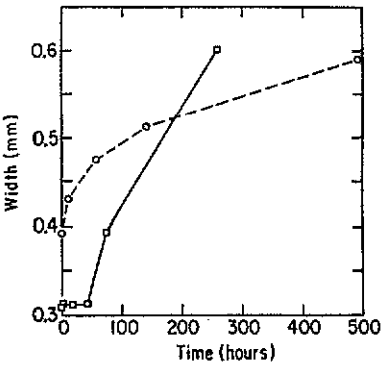

Figure 11. Plateau border broadening. Plateau border widths versus time for two different two-dimensional soap froth experiments conducted in sealed cells. From Glazier and Stavans (1989).

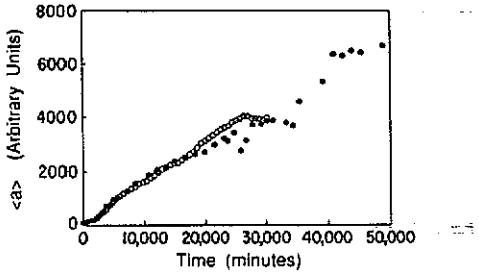

Figure 12. Area growth in soap froth. Average area $\langle a \rangle$ versus time for a dry two-dimensional soap froth in a large container (●), and for the two-dimensional next-nearest-neighbour square-lattice Potts model (○). From Glazier *et al* (1990a).

10. Recent experiments

The experiments discussed in section 9 yielded values for β ranging from 0.32 to 1.0 (a surprisingly large range for a simple parameter), and suggested that the soap froth both did and did not reach a scaling state. Recent theories and simulations have clarified the situation and confirmed the existence of a scaling state with $\beta = 0.5$. Stavans and Glazier (1989) showed that $\rho(n)$ reached constant form values regardless of initial conditions, so that the long-term state of the soap froth was a scaling state (see figure 10). Glazier and Stavans (1989) suggested that the anomalous value of β resulted from the growth of the PB during coarsening (see figure 11). Later Weaire and Bolton (1990), Bolton (1990) and Weaire (1991, 1992) showed theoretically (as discussed in section 15) that PB could explain the measured value of β.

When Glazier *et al* (1990a) studied coarsening in a dry froth in a much larger cell, they obtained $\beta = 0.5$ (see figure 12). They also verified that $\rho(n)$ and $\rho(a/\langle a \rangle)$ were constant in long-time states. Stavans (1990) performed experiments in a drained experimental cell, in which he periodically removed fluid from the froth to keep the widths of the PB narrow and constant at $(5 \pm 1.5)\%$ of the spacing between his top and bottom plates. He found $\beta = 0.5$ within a few per cent at all times.

Table 3. Growth exponent ($\langle r \rangle \propto t^{\beta}$) for soap froth, lipids, magnetic bubbles, metals and models.

System	β	Reference
Soap froth	0.5	Smith (1952)
Soap froth	1.0	Aboav (1970)
Soap froth (wet)	0.32	Glazier *et al* (1987)
Soap froth (dry)	0.5	Glazier *et al* (1990a)
Soap froth (drained)	0.5	Stavans (1990)
Soap froth (3D)	0.5	Durian *et al* (1990)
Lipid monolayer (wet)	0.3	Berge *et al* (1990)
Lipid monolayer (intermediate)	0.4	Stine *et al* (1990)
Lipid monolayer (dry)	0.5	Berge *et al* (1990)
Magnetic froth	None	Molho in Glazier (1989)
Magnetic froth (high B)	1.45	Babcock *et al* (1990)
Al	0.25	Gordon and El-Bassyouni (1965)
Co_3Ti	0.34	Takasugi and Izumi (1985)
Fe	0.40	Hu (1974)
Pb	0.40	Bolling and Winegard (1958)
Sn	0.50	Holmes and Winegard (1959)
MgO	0.5	Kapadia and Leipold (1974)
Direct simulation	0.5	Weaire and Kermode (1984)
Direct simulation	0.5	Frost *et al* (1988)
Direct simulation	0.5–0.6	Herdtle and Aref (1991b)
Lifschitz–Slyozov	0.33	Lifschitz and Slyozov (1959)
Mean-field theory	0.5	Fradkov *et al* (1985b)
Vertex model (2D)	0.5	Fullman (1952)
Vertex model (3D)	0.5	Nagai *et al* (1990)
Potts model (2D)	0.5	Grest *et al* (1984)
Potts model (3D)	0.5	Anderson *et al* (1989)

11. Direct simulation of two-dimensional froths

In the following sections we discuss a few of the many attempts to simulate two-dimensional grain growth. These fall into several classes: direct simulations, mean-field theories, vertex models and the Potts model. We will not discuss the many statistical models that predict $\rho(n)$ and $\rho(a/\langle a \rangle)$ in the scaling state but do not determine the coarsening dynamics.

Direct simulations attempt to reproduce accurately the equilibrium configuration of a froth with a model that includes the essential physics of gas diffusion and wall motion. They also include rules for the changes of topology that take place whenever cells or cell sides shrink to zero size. Since topological changes have not been modelled dynamically in a disordered froth (such modelling has been done in a regular hexagonal lattice by Kraynik and Hansen (1986) and Kraynik (1988)), these are treated as sudden transitions between quasi-static configurations. In these models, it is easy to include impurity pinning to obtain the lower scaling exponents observed in metals (see table 3; Frost and Thompson 1986, Thompson *et al* 1987).

Frost and Thompson took a metallurgical approach in their simulations and assumed that grain boundaries had a fixed mobility μ, so that the velocity of any point on the boundary was

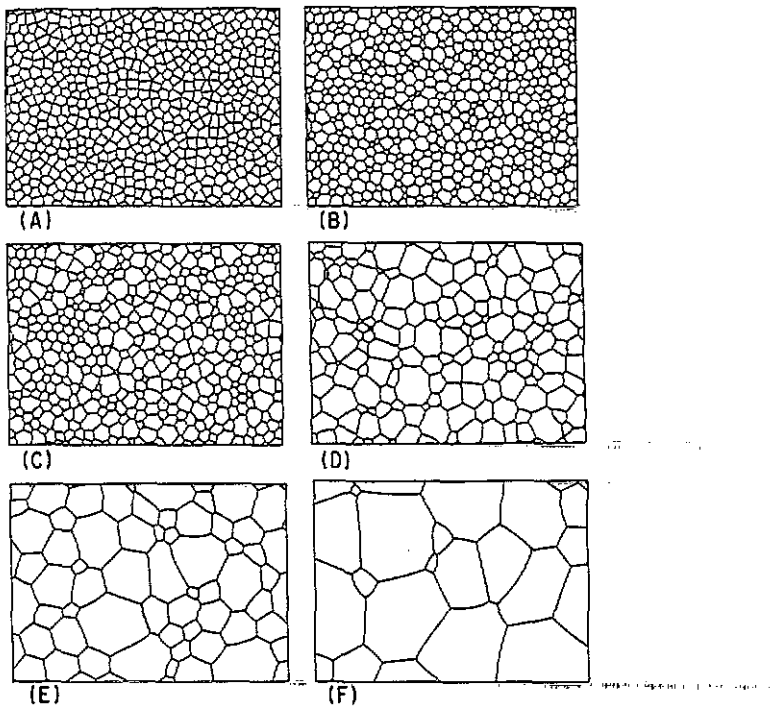

Figure 13. Pattern evolution in a direct simulation: (A) Initial excluded-volume Voronoi construction; (B) $t = 0.5$ diffusion times; (C) $t = 1.0$ diffusion times; (D) $t = 3.0$ diffusion times; (E) $t = 10.0$ diffusion times; (F) $t = 30.0$ diffusion times. From Frost *et al* (1988).

$$v(x) = \mu\hat{n}/\rho(x) \tag{17}$$

where $\rho(x)$ is the local curvature and $v(x)$ the local velocity at a point x on the boundary, and $\hat{n}$ the unit normal at that point. In this model, as discussed in section 5, the individual grains need not have well defined pressures. The boundaries were divided into nearly flat segments, which were approximated by circular arcs, and evolved according to equation (17). Extra segments were added as needed, and the positions of vertices adjusted to produce 120° angles. Topological changes were made in a separate step. Using this model, Frost and Thompson carried out extremely long simulations, yielding $\beta = 0.5$ to high accuracy over a three-decade increase of pattern length scale (Frost and Thompson 1986, 1987a, Frost *et al* 1988, Howe 1987, Thompson *et al* 1987). We show the pattern evolution of this model in figure 13.

The models of Kermode and Weaire (1990), Wejchert *et al* (1986), Weaire and Kermode (1983a, b) and Aref and Herdtle (1990) are similar in spirit but differ in technique (Herdtle and Aref 1991b). Weaire and Kermode (see figure 14) relaxed their pattern to equilibrium by a repeated cycle of *local* adjustments, while Herdtle and Aref performed simultaneous adjustments on the entire structure. This may be significant, since the soap froth is a strictly chaotic system (topological redistribution represents a repeated approach to sensitive choice points), so that the detailed evolution of the pattern may depend on the sequence in which adjustments are made. However, since

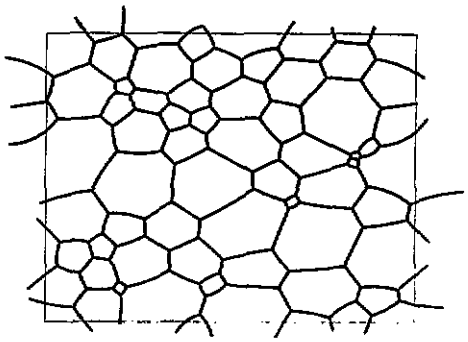

Figure 14. Scaling state soap froth pattern in a direct simulation. From Weaire and Kermode (1983b).

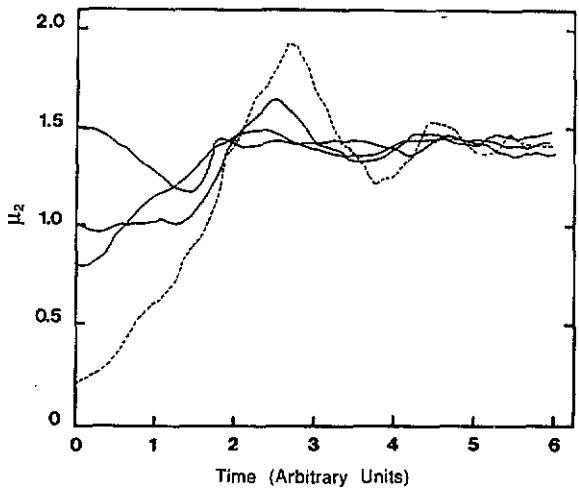

Figure 15. Evolution of μ_2 versus time in a direct simulation for varying initial conditions. From Weaire and Lei (1990).

both authors separate topological adjustments from diffusive adjustments, the probability of such discrepancies is minimized.

Herdtle and Aref (1991b) point out that there are many initial conditions for which a scaling state is never reached, or for which the approach to a scaling state takes an arbitrarily long time. Pathological examples of the former case include a tessellation of regular squares and octagons with a small compression in one direction, which retains its initial $\rho(n)$ at all times (note that this pattern is unstable to small perturbations), and of the latter a large perfect hexagonal lattice with a single defect. The tacit assumption is that in experiments the initial condition is such that a statistical treatment is appropriate, and that such pathological conditions will not arise spontaneously.

Weaire and Lei (1990) obtained the asymptotic value of $\mu_2 = 1.42 \pm 0.05$, using several samples of 500 cells, with differing initial structures (see figure 15). The variation of mean cell area with time was consistent with $\beta = 0.5$ (Lei 1990). Herdtle and Aref (1991a), using samples of 1024 cells, obtain $\mu_2 = 1.2$ and, more disturbingly, $0.5 < \beta \leqslant 0.6$, with the difference from 0.5 regarded as significant.

The difference in the values of μ_2 may be due to the way in which very small cells are treated in the simulations. Such cells, though short-lived, contribute disproportionately

to μ_2, so that it matters whether they have, say, three or four sides. However, there is a much greater discrepancy in the early-time behaviour, with Weaire and Lei reproducing the experimentally observed 'overshoots' of the experimental data while Herdtle and Aref do not. The origin of this disagreement remains a puzzle.

12. Mean-field theories

Direct simulations decompose coarsening into two processes, a law defining the rate of change of area of a bubble, and a set of scattering processes that occur when bubbles disappear. We may simplify our models by applying these processes directly to the distribution functions (with or without correlations), to obtain mean-field theory of master equation type. The typical form is

$$d\rho(n, a, t)/dt \propto (da/dt)(n - 6)\rho(n, a, t). \tag{18}$$

There were many early attempts to write such models for metallic grain growth using growth laws based on bubble radius (see Glazier 1989 for a discussion). These were unsuccessful because, as discussed in section 5, radius-based models yield $\beta = 0.33$. On the other hand, any von Neumann-based mean-field theory will yield $\beta = 0.5$, according to equation (14). Mean-field theories also treat bubble disappearance (T2 processes) and stress relaxation (T1 processes) separately, so the rate of T1 processes appears as a free parameter (generally set equal to zero).

Fradkov *et al* (1985a, b, 1987, 1988), Beenakker (1986, 1987, 1988) and Marder (1987) all studied von Neumann's law mean-field theories. The first two also looked at evolution on a topological network. In these models the topology and connectivity of the network are preserved but the positions of the vertices are neglected, to produce a network of vertices (representing bubbles) with an area at each vertex and an associated list of neighbours. The areas are then evolved according to von Neumann's law. Vertices are deleted and the topology rearranged according to the allowed scattering processes, whenever a vertex reaches zero area. These models reproduced the transients observed experimentally for initially ordered patterns (see figure 16) and gave distribution functions with the correct exponential cut-offs, but the wrong shapes. Recently Stavans *et al* (1991) have shown that the error in the distribution functions was due to incorrect choices for the correlations of side redistribution on bubble disappearance.

13. Vertex models

Another approach to a direct simulation was originally proposed by Fullman (1952), and has been extensively pursued by Kawasaki and co-workers (see figures 16 and 17) (Kawasaki *et al* 1989, Kawasaki 1990, Kawasaki and Enomoto 1988, Enomoto and Kato 1990, Nakashima *et al* 1989, Nagai *et al* 1988, 1990). In this case the vertices at which bubbles meet are treated as pseudo-particles with well defined mobilities and subject to forces determined by the positions of the neighbouring vertices. The connections between the vertices are assumed to be straight and deviations from 120° angles are used to determine an effective curvature. The great advantage of this method is that it is computationally efficient. Fullman did his computations by hand, and his original model

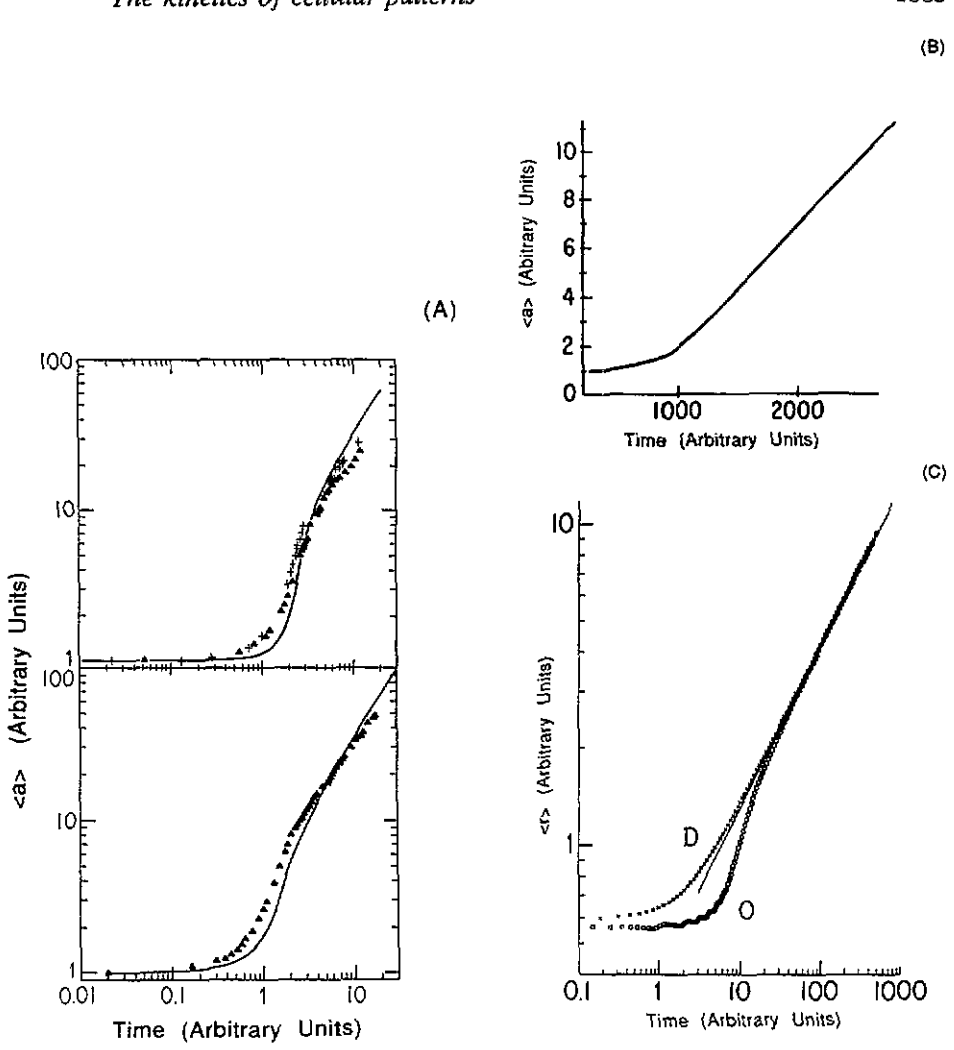

Figure 16. Average area versus time for mean-field theories. (A) From Marder (1987); full curves show simulation, triangles are data of Glazier *et al* (1987). (B) From Fradkov *et al* (1985b). (C) From Beenakker (1988), showing the different transients for initially ordered (O) and initially disordered (D) patterns.

is one of the simplest and most intellectually satisfying. The effective force is simply the sum of unit vectors connected to the three neighbours j of a vertex, x_i:

$$F_i = \sum_{\text{neighbours } j} (x_i - x_j)/|x_i - x_j|. \tag{19}$$

The vertex velocity v_i is determined from the force by assuming a boundary-length-dependent mobility:

$$v_i = F_i |F_i| / \sum_{\text{neighbours } j} F_i \cdot (x_i - x_j). \tag{20}$$

However, there is no rigorous way to convert true curvatures into vertex angles, so

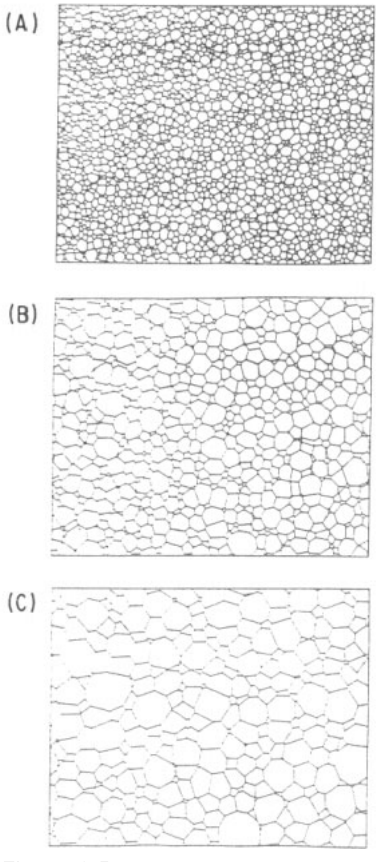

Figure 17. Pattern evolution of a vertex model simulation: (A) 5.0 Monte Carlo steps; (B) 20 Monte Carlo steps; (C) 50 Monte Carlo steps. Redrawn from Kawasaki *et al* (1989).

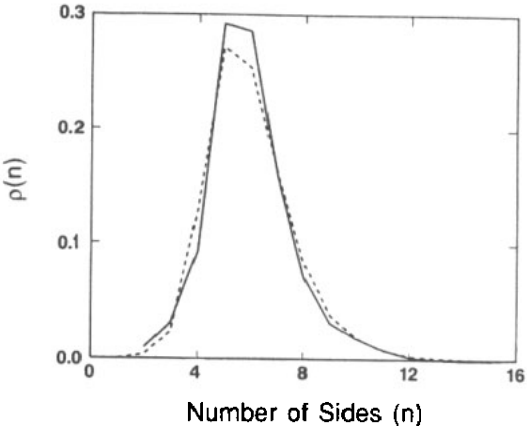

Figure 18. Scaling state topological distributions for a two-dimensional soap froth (——) and a nearest-neighbour hexagonal-lattice Potts model (– – – –). From Glazier *et al* (1990a).

vertex models remain unsystematic approximations. Kawasaki and collaborators have studied many variations of this basic model. They all reach a scaling state with $\beta = 0.5$, but do not obey von Neumann's law, and their scaling state distributions generally differ significantly from experimental results.

14. The Potts model

The two-dimensional Potts model simulation is another extensively studied model for coarsening in two dimensions (Anderson *et al* 1984, 1985, 1989, Grest *et al* 1984, 1992, Srolovitz *et al* 1984, Glazier *et al* 1990a, b, Holm *et al* 1991). It is fundamentally a microscopic metallurgical approach to coarsening, with 'atoms' that jump from grain to grain. Since there is an underlying lattice, there is an underlying length scale, which has created some uncertainty in the past over the validity of simple dimensional arguments.

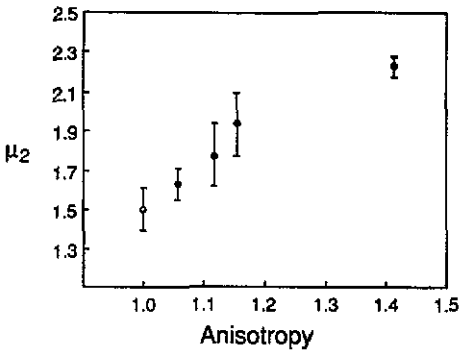

Figure 19. Plot of μ_2 versus anisotropy for the scaling state distributions of two-dimensional Potts model simulations. From Holm *et al* (1991).

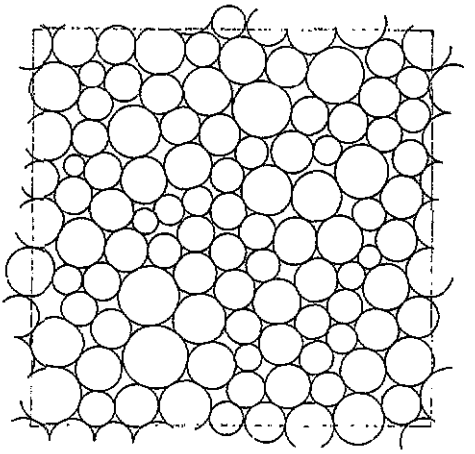

Figure 20. Simulation of soap froth with large Plateau borders. Compare to the lipid monolayers shown in figure 23(A). From Bolton and Weaire (1992).

The model itself consists of a surface energy term. There are an arbitrary number of equivalent spin states $\sigma(i, j)$ located on a regular lattice. The basic Hamiltonian is

$$\mathcal{H} = \sum_{(i,j)(i',j') \text{ neighbours}} 1 - \delta_{\sigma(i,j),\,\sigma(i',j')}. \tag{21}$$

Evolution proceeds by selecting a spin at random and converting it to another value with probability $\exp(-\Delta\mathcal{H}/kt)$, where $\Delta\mathcal{H}$ is the energy gain produced by the change. Above a temperature T_c, the pattern melts into random disordered spins. Below T_c, the spins coalesce into well defined patches, with each different spin state denoting a different grain. At $T = 0$ the domains grow relaxationally as in soap froth.

There are two basic differences between the Potts model and the soap froth. The time for diffusion along a grain boundary in the Potts model is long compared to the diffusion time across the boundary as in a metal. Thus boundaries in the Potts model and metals are not equilibrated. Also, the Potts model, like a metal, has a lattice anisotropy while the soap froth is entirely isotropic.

Holm *et al* (1991) have studied the effect of lattice anisotropy on coarsening. Short-range (high lattice anisotropy) interactions produce pinned patterns rather than continuously coarsening scaling states. However, the nearest-neighbour hexagonal and next-nearest-neighbour square-lattice Potts models reach scaling states with $\beta = 0.5$ and $\mu_2 < 2.0$, with μ_2 and the duration of the transient increasing monotonically with the anisotropy (see figures 18 and 19). Extrapolating to zero lattice anisotropy gives the measured value for the soap froth, while the high-anisotropy limit agrees with the experimental result of Fradkov *et al* (1985a) for two-dimensional grain growth in Al + 10^4 Mg foil at 460 °C. In metals, the effective β increases with the annealing temperature (which is equivalent to a decreasing anisotropy) to a maximum of 0.5 near the melting point (Beck 1954).

15. Plateau borders

In this and the following sections we consider extensions to ideal two-dimensional soap froth coarsening: PB, three-dimensional froths, lipid monolayers and magnetic domains.

All of the models that we have reviewed treat bubbles that are separated by lines meeting at point vertices. As we noted, several aspects of the coarsening of two-dimensional soap froths were inconsistent with such models. In metals, it was known that during coarsening impurities initially distributed uniformly in the material tend to segregate preferentially in the grain boundaries, reducing the boundary mobility (which is roughly equivalent to the von Neumann κ') and resulting in a lower effective β (Beck 1954).

In the soap froth, vertices consist of fluid-filled triangular regions or PB. If coarsening takes place in a sealed cell, the size of the PB increases, as the total boundary length shrinks, preserving the total fluid volume. If the PB size is much larger than the cell wall thickness, the latter can be treated as infinitesimal and each PB takes the form of a 'triangle' with curved sides. We may assign a pressure p_0 to the fluid within the triangle, and the pressure difference between this fluid and an adjoining cell determines the curvature of that side of the PB, in equilibrium with surface tension:

$$p_i - p_j = \tfrac{1}{2}\sigma c \tag{22}$$

agreeing with equation (4) except that the surface tension is one-half that of a bubble wall because the latter has two sides. Equilibrium also requires that the PB connect smoothly (i.e. with a common tangent) to cell walls.

Using elementary mechanical arguments, Bolton and Weaire (1991) showed that the modelling of PB can be drastically simplified. Provided only three-sided PB occur, the circular extrapolations of the bubble walls into the PB meet in a common point at 120°. Thus the PB may be regarded as decorations superimposed on an undisturbed equilibrated froth structure. Using this result, and computations in which 'decoration' of the skeletal structure with PB was included, it was possible to explain the observed angle, von Neumann's law and β deviations. The structure shown in figure 3 was produced by this method.

As far as diffusion and coarsening are concerned, the PB simply reduce wall lengths and hence diffusion rates as originally suggested by Glazier and Stavans (1989), in accordance with equation (3). The chief surprise was that a decrease in κ' too small to measure experimentally could still have a large effect on the measured value of β.

Bolton and Weaire assumed a uniform PB pressure, since the PB connect at the top and bottom plates of the apparatus. A more detailed consideration of the effects of PB on coarsening would have to analyse the variation of this pressure (and hence the size of the PB) with time, in accordance with particular experimental conditions.

The assumption that all PB are three-sided restricts this picture to low fluid fractions. If the proportion of fluid is increased, fourfold and higher-order vertices are formed. This regime occurs in lipid monolayers, and has been explored in direct simulations by Bolton and Weaire (1992) (see figure 20), with regard to mechanical properties but not coarsening behaviour.

16. Three dimensions

In three dimensions the average total curvature of the surface of a bubble is not determined by its number of faces (Avron and Levine 1992). Thus there is no simple three-dimensional equivalent of von Neumann's law. In a two-dimensional pattern the average number of sides per grain is six. In three dimensions there is an extra degree of freedom, so the equations for the number of faces per grain are under-determined. If the average

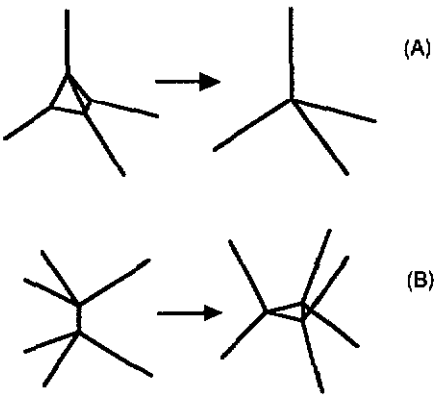

Figure 21. Topological transformations in three dimensions: (A) T2(4) process; (B) T1 process.

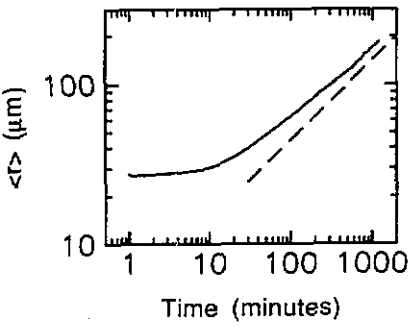

Figure 22. Three-dimensional growth of area versus time in shaving cream. From Durian *et al* (1990b).

number of faces per grain is $\langle f \rangle$ and the average number of sides per face is $\langle n_f \rangle$, then for an infinite froth the quantities are related as

$$\langle n_f \rangle = 6 - 12/\langle f \rangle. \tag{23}$$

Rivier, by analogy with von Neumann's law, has suggested that a possible law for the dynamics could be

$$\mathrm{d}v_f/\mathrm{d}t = \kappa(\langle f \rangle - f) \tag{24}$$

where v_f is the volume of a bubble with f faces and $\langle f \rangle$ is the average number of faces per bubble in the froth, but his argument is at best an approximation true for ensembles, unlike von Neumann's law, which should hold for individual grains. Because of the difficulty of experiments in three dimensions, this relation has not yet been experimentally tested.

The basic topological transformations are also different, though all changes can still be reduced to two basic cases: the T1 process in which two bubbles push together to create a new face (figure 21(B)) and the T2(4) process, the disappearance of a tetrahedral grain (figure 21(A)). However, the three-dimensional T1 process does not conserve the total number of faces. It is also unclear how many different types of polyhedral bubbles can disappear directly without side shedding and thus how many different types of T2 processes there are. However, regardless of the detailed form of the equation, in a scaling state, the curvature must depend only on the bubble size and dimensionless parameters. The rate of diffusion is proportional to the surface area times the reciprocal of the radius of curvature with a constant depending on dimensionless parameters:

$$\mathrm{d}v/\mathrm{d}t = \kappa''(1/r)a \qquad [\mathrm{m}^3\,\mathrm{s}^{-1}] = \kappa''[\mathrm{m}^{-1}][\mathrm{m}^2] \qquad \Rightarrow \qquad \kappa'' \propto [\mathrm{m}^2\,\mathrm{s}^{-1}]. \tag{25}$$

Thus by equation (14), $\beta = 0.5$ and $\langle v \rangle \propto t^{1.5}$.

Nagai *et al* (1990) wrote a vertex model assuming that only tetrahedral bubbles disappear directly and began with a Voronoi construction containing 343 grains. Their equation of motion is of a Fullman type with a fixed mobility per vertex σ:

$$\frac{\mathrm{d}\boldsymbol{r}_i}{\mathrm{d}t} = \tfrac{1}{2} \sum_{\Delta_\tau \text{ around vertex}} \sigma \boldsymbol{n}_\tau \times (\boldsymbol{r}_j - \boldsymbol{r}_k) \tag{26}$$

where Δ_τ is a triangle (i, j, k) containing vertex i, $\boldsymbol{n}_\tau$ the clockwise unit normal to (i, j, k)

and r_j the position of the vertex j. They obtained a scaling value of $\langle f \rangle = 13.6$ and $\beta \simeq 0.5$, determining their scaling regime by direct measurements of $\rho(f)$ and $\rho(v/\langle v \rangle)$. They also compared the results for two-dimensional sections of their model to those obtained for two-dimensional simulations and experimental two-dimensional sections of metals and found substantial differences. Nor did they find good agreement between their model and the three-dimensional Potts model or actual metal grains. Since the derivation of the law of motion for for vertices is inevitably *ad hoc*, a three-dimensional version of von Neumann's law is needed to check the realism of the model. Avron and Levine (1992) have recently made progress towards such a model.

While the computational burden for three-dimensional $Q = 48$ Potts model calculations is substantially greater than in two dimensions, Anderson *et al* (1989) have performed three-dimensional simulations on a $100 \times 100 \times 100$ lattice using a variety of interaction distances at zero temperature. Their technique was identical to that described for the two-dimensional case. For nearest neighbour interactions, they found that grain growth ceased after a short time. For next-nearest-neighbour interactions they did not reach a scaling state, though the pattern continued to coarsen with an effective $\beta = 0.28 \pm 0.02$. For longer-range interactions they reached a scaling state with $\beta = 0.48 \pm 0.04$. However, a naive fit to their data gives $\beta = 0.39 \pm 0.02$. Thus, the effective β was strongly dependent on the time cut-offs used in the fit, which may be biased by the expectation that $\beta = 0.5$. They found $\langle f \rangle = 12.9$ for the final scaling state. The agreement with experimental values for metal grains was good (both the experimental and simulational $\rho(v/\langle v \rangle)$ are essentially log-normal (Kurtz and Carpay (1981)) with the residual discrepancy compatible with anisotropy effects.

The experimental difficulties of direct measurements of three-dimensional structure are substantial, both in information storage and practicalities like measuring time. The only direct measurement of the topology of a soap froth, unfortunately, was made on a froth in which all bubbles had the same volume and it was assumed that no grain growth occurred (Matzke 1945, 1946, Matzke and Nestler 1946)! In metals, serial sectioning gives the length scale easily, though $\rho(f)$ and $\rho(v/\langle v \rangle)$ are difficult to determine. The value of β fluctuates between 0.25 and 0.5 as shown in table 3, apparently due to impurity and anisotropy effects.

Recently Durian *et al* (1990, 1991a, 1991b) have carried out a series of experiments using diffusing-wave spectroscopy on the evolution of Gillette Foamy Regular shaving cream. This is produced as a homogeneous froth of very small bubbles (diameter of 10 to 20 μm), with no large gaps. During their experiment they observed no gravitational drainage or wall breakage. Their technique allows them to measure the mean distance between scatterings by bubble films. After a short transient (during which the rate of evolution increased monotonically to its final vaolue) they found $\beta = 0.47 \pm 0.05$ (see figure 22). Unfortunately, while their technique allowed them to estimate the total rate of side redistribution in the froth, it did not allow them to measure $\rho(f)$.

17. Lipid monolayers

In a lipid monolayer system, a monolayer of an amphiphilic molecule (e.g. pentadecanoic acid) is floated on a water surface. The monolayer can undergo a phase transition between a two-dimensional gas phase and a two-dimensional liquid phase. The two phases may be observed directly using a fluorescent amphiphilic dye, which fluoresces only in the liquid phase (Lösche and Möhwald 1984). When the pressure is gradually

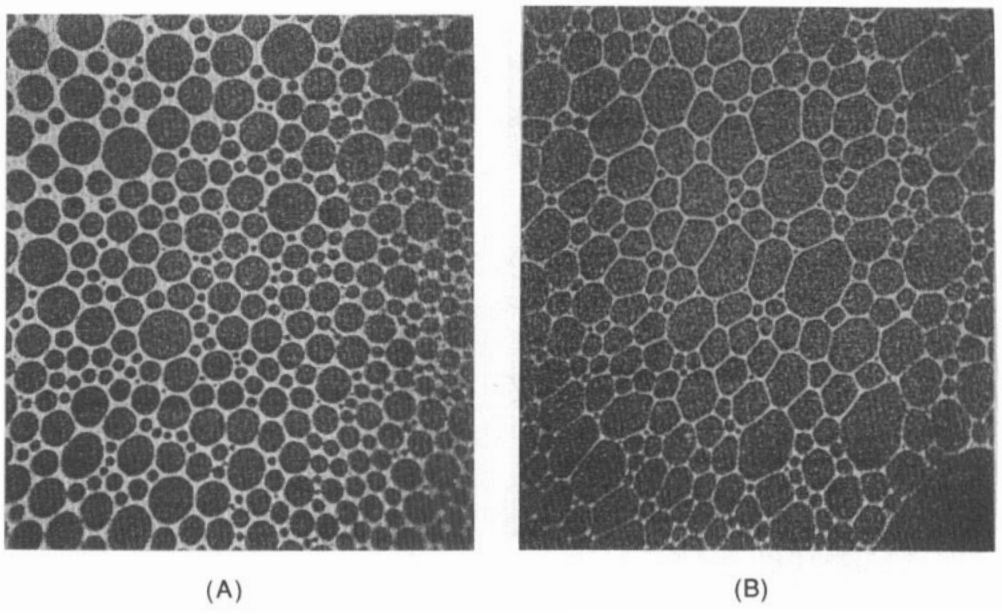

Figure 23. Bubbles in lipid monolayers: (A) separated; (B) close-packed. Figure supplied by Berge (1989).

increased through the phase transition, small bubbles of gas form, surrounded by a continuous background of liquid. Sometimes the gas bubbles contain small liquid drops, but these do not seem to affect the subsequent evolution. The basic topology is identical to that of the soap froth, except that the liquid and gas are composed of the same material, so there need be no conservation of their amounts. The liquid fraction is thus an easily tunable parameter, allowing the creation of patterns ranging from single isolated round gas bubbles (figure 23(A)) to fully polygonal close-packed bubbles (figure 23(B)).

The existence of dipole–dipole interactions prevents the lipid bubbles from coalescing and allows for the formation of both bubble and stripe patterns as in magnetic bubbles (Andelman *et al* 1987). The chief difference from magnetic bubbles is that the dipole interaction appears to be short-range. So, for widely separated bubbles, it is most convenient to think of the interaction between the bubbles and a background mean field. This is the limit originally proposed for grain growth by Lifschitz and Slyozov (equation (13)), which yields $\beta = 0.33$. Berge *et al* (1990) found $\beta = 0.3$ for a separated froth of round bubbles (liquid fraction 50%), with a power-law tail in the area distribution function, different from the soap froth's exponential cut-off.

In the close-packed limit, local interactions should dominate to produce von Neumann's law behaviour, with $\beta = 0.5$ and soap-froth-like distributions. Experimentally, Berge *et al* found, in the close-packed case (liquid fraction 25%), $\beta = 0.5$ and soap-froth-like distribution functions, with $\mu_2 = 1.4$. Stine *et al* (1990), working with an intermediate fluid fraction, found $\beta = 0.4$ and $\mu_2 = 1.95 \pm 0.6$, with $\rho(n)$ and $\rho(a/\langle a \rangle)$ intermediate between Berge *et al*'s two results. It appears that in the lipid monolayer β can vary smoothly between 0.33 and 0.5.

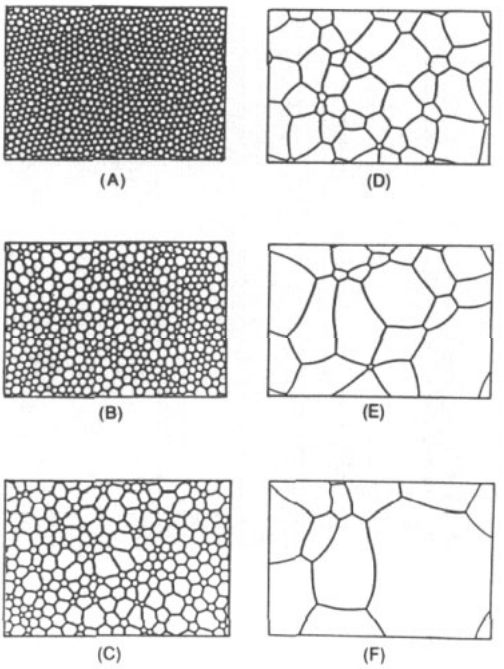

Figure 24. Evolution of a magnetic froth with increasing ((A) → (F)) applied magnetic field. Figure supplied by Molho (see Glazier 1989).

If we assume that the filling fraction is constant during the experiment, the simplest combination of the two growth laws is:

$$da(n, r)/dt = \varepsilon\kappa(n - 6) + (1 - \varepsilon)\kappa(\langle 1/r\rangle - 1/\langle r\rangle) \tag{27}$$

where ε increases from 0 to 1 with the filling fraction. So far, there does not appear to have been any study of such intermediate mean-field theories.

18. Magnetic domains

Magnetic froth in a garnet film presents a subtler problem. That garnet films can produce froths that coarsen with increasing magnetic fields has been known for a long time (Wolfe and North 1974). More recently, they have been studied by Babcock and Westervelt (1989a, b, 1990) and Molho (Glazier 1989, Weaire *et al* 1991). The differences from normal coarsening are striking. While the pattern energy does contain a term proportional to the total boundary length in the froth, for all but weak fields, the dominant term is the dipole interaction between patches of bulk magnetization. An external magnetic field applied to favour one direction of magnetization sets the balance between the two terms, and hence a length scale. The patterns are static, with the applied field playing the role of time (figure 24). The presence of dipole fields causes the walls to repel each other, stabilizing small bubbles and leading to patch-wise, abrupt evolution. Babcock *et al* (1990) found a scaling regime for large magnetic fields with $\beta = 1.45$. Molho (see Glazier 1989), on the other hand, found no scaling state or power-law growth

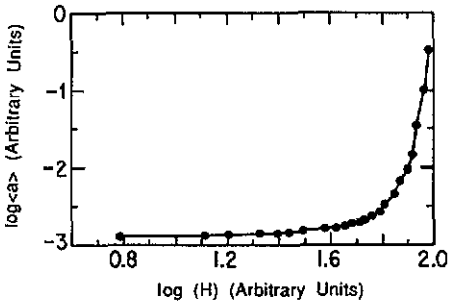

Figure 25. Average area versus applied magnetic field for a magnetic froth. From Glazier (1989).

with increasing applied magnetic field (figure 25). The origin of this discrepancy remains to be explained.

Weaire *et al* (1991) have approached the problem by treating the long-range interaction as a perturbation to a direct simulation soap froth model, where the wall energy depends on the areas of the neighbouring bubbles only out to a defined range (figure 26). Using nearest- and next-nearest-neighbour interactions gives the correct qualitative loss of stability for few-sided bubbles, and reasonable values for $\rho(n)$ and area growth. It also gives the observed stabilization of small bubbles followed by patch-wise evolution. It cannot, however, create the more exotic labyrinths and other textures that characterize magnetic bubbles. Higher-order models might.

19. Conclusions

It now seems that Smith's (1952) original result was correct: the two-dimensional soap froth reaches a scaling state with $\beta = 0.5$. This state is characterized by well defined distributions with $\mu_2 = 1.5$. By implication, any other isotropic two-dimensional pattern that obeys von Neumann's law and has only T1 and T2 topological processes will have the same values of β and μ_2. Examples include low-liquid-fraction lipid monolayers and grain growth in metal films at high temperatures. Where secondary effects like growing Plateau borders, impurity pinning, bubble stabilization, or anisotropy are important, the values of β and μ_2 may change. Similarly, changes in the underlying topological processes (e.g. cell division in biology) or the presence of higher-order vertices, or changes in the underlying dynamics (e.g. the Lifschitz–Slyozov law) can change β and μ_2.

Why did it take so long to reach such a seemingly obvious result? The origin of the confusion was twofold. First, the transients in a soap froth can be very long. Many finite systems do not reach a scaling state until they contain only a few cells. Moreover, these transients can mimic power-law growth. Secondly, rather subtle details can produce large changes in the measured β for both experiments (PB) and models (anisotropy). The moral seems to be that it is difficult indeed to identify scaling states, especially from the exponents alone, and that it is very difficult to disentangle the generic behaviour of a froth from artifacts caused by the details of experimental design. In the case of three-dimensional bubbles, this lesson seems to have been learned. There is universal agreement that $\beta = 0.5$.

However, now that the baseline behaviour of the two-dimensional soap froth is understood, it is possible to add complications in a controlled manner. The recent studies

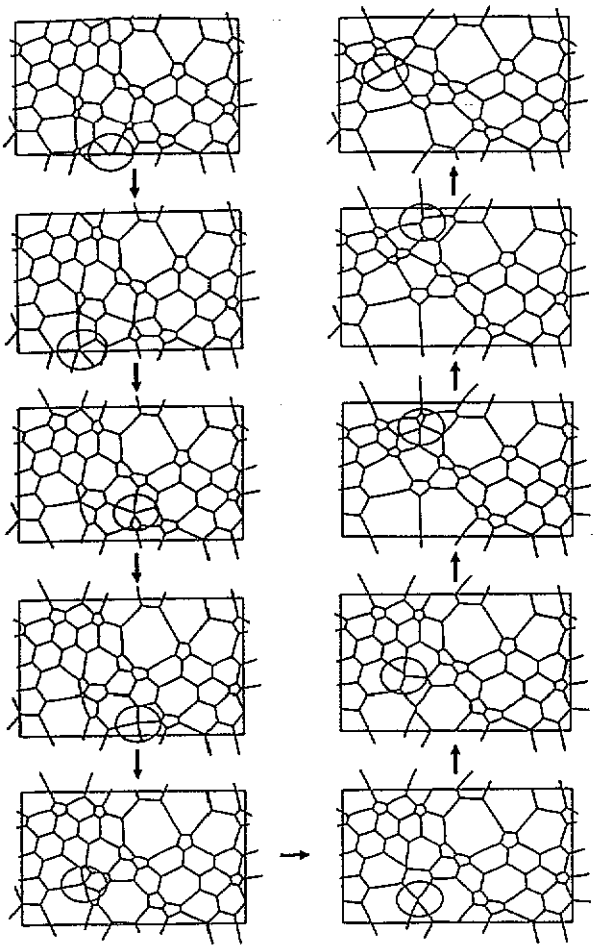

Figure 26. Direct simulation of the cascade of topological transformations resulting from a small change in effective magnetic field. From Weaire *et al* (1991).

of PB, lipid monolayers, three-dimensional bubbles and magnetic froths all owe their existence to Smith's original insight that the soap froth offered an appealing analogue to ideal grain growth.

Acknowledgments

JAG wishes to thank Trinity College, Dublin, for hospitality and support, and JSPS (Japan Society for the Promotion of Science) for research support. DW wishes to acknowledge the research support of EOLAS (Irish Science and Technology Agency).

References

Abbruzzese G (ed) 1992 *Proc. Int. Conf. on Grain Growth in Polycrystalline Materials (Rome)* at press

Aboav D A 1970 *Metallography* **3** 383
Almgren F J and Taylor J E 1976 *Sci. Am.* **235** 82
Andelman D, Broçhard F and Joanny J-F 1987 *J. Chem. Phys.* **86** 3673
Anderson M P, Grest G S and Srolovitz D J 1985 *Scr. Metall.* **19** 225
—— 1989 *Phil. Mag.* B **59** 293
Anderson M P, Srolovitz D J, Grest G S and Sahni P S 1984 *Acta Metall.* **32** 783
Aref H and Herdtle T 1990 *Topological Fluid Mechanics* ed H Moffat and A Tsinober (Cambridge: Cambridge University Press) p 745
Atkinson H V 1988 *Acta Metall.* **36** 469
Avron J E and Levine D 1992 *Phys. Rev. Lett.* submitted
Babcock K L, Seshadri R and Westervelt R M 1990 *Phys. Rev.* A **41** 1952
Babcock K L and Westervelt R M 1989a *Phys. Rev. Lett.* **63** 175
—— 1989b *Phys. Rev.* A **40** 2022
—— 1990 *Phys. Rev. Lett.* **64** 2168
Beck P A 1954 *Adv. Phys.* **3** 245
Beenakker C W J 1986 *Phys. Rev. Lett.* **57** 2454
—— 1987 *Physica* A **147** 256
—— 1988 *Phys. Rev.* A **37** 1697
Berge B 1989 unpublished
Berge B, Simon A J and Libchaber A 1990 *Phys. Rev.* A **41** 6893
Bolling G F and Winegard W C 1958 *Acta Metall.* **6** 283
Bolton F and Weaire D 1990 *Phys. Rev. Lett.* **65** 3449
—— 1991 *Phil. Mag.* B at press
—— 1992 *Phil. Mag.* B at press
Bragg L and Nye J F 1947 *Proc. R. Soc. Lond.* A **190** 474
Brook R J 1976 *Ceramic Fabrication Processes (Treatises on Materials Science and Technology 9)* ed F F Y Wang (New York: Academic) p 331
Durian D J, Weitz D A and Pine D J 1990 *J. Phys.: Condens. Matter* **2** SA433
—— 1991a *Science* **252** 686
—— 1991b *Phys. Rev.* A at press
Enomoto Y and Kato R 1990 *Acta Metall. Mater.* **38** 765
Fradkov V E, Kravchenko A S and Shvindlerman L S 1985a *Scr. Metall.* **19** 1291
Fradkov V E, Shvindlerman L S and Kris R E 1988 *Phil. Mag. Lett.* **58** 670
Fradkov V E, Shvindlerman L S and Udler D G 1985b *Scr. Metall.* **19** 1285
—— 1987 *Phil. Mag. Lett.* **55** 289
Frost H J and Thompson C V 1986 *Computer Simulation of Microstructural Evolution* (Warrendale, PA: The Metallurgical Society) p 33
—— 1987a *Acta Metall.* **35** 529
—— 1987b Modeling of optical thin fibres *Proc. SPIE: Int. Soc. Opt. Eng.* ed M R Jacobson **821** 77
Frost H J, Thompson C V, Howe C L and Whang J 1988 *Scr. Metall.* **22** 65
Fu T 1988 *MS Thesis* Trinity College, Dublin
Fullman R L 1952 *Metal Interfaces* (Cleveland, OH: American Society for Metals) p 179
Gardner M 1986 *Sci. Am.* **254** 16
Getis A and Boots B 1978 *Models of Spatial Processes: An Approach to the Study of Point, Line and Area Patterns* (Cambridge: Cambridge University Press)
Glazier J A 1989 *PhD Thesis* University of Chicago
Glazier J A, Anderson M P and Grest G S 1990a *Phil. Mag.* B **62** 615
Glazier J A, Grest G S and Anderson M P 1990b *Simulation and Theory of Evolving Microstructures* ed M P Anderson and A D Rollet (Warrendale, PA: Minerals, Metals and Materials Society) p 41
Glazier J A and Stavans J 1989 *Phys. Rev.* A **40** 7398
Gordon P and El-Bassyouni T A 1965 *Trans. Am. Inst. Min. Eng.* **233** 391
Grest G S, Glazier J A, Anderson M P, Holm E A and Srolovitz D J 1992 unpublished
Grest G S, Srolovitz D J and Anderson M P 1984 *Phys. Rev. Lett.* **52** 1321
Herdtle T and Aref H 1991a *J. Fluid Mech.* at press
—— 1991b *Phil. Mag. Lett.* at press
Holm E, Glazier J A, Srolovitz D and Grest G S 1991 *Phys. Rev.* A **43** 2662
Holmes E L and Winegard W C 1959 *Acta Metall.* **7** 411
Howe C L 1987 *ME Thesis* Dartmouth College

Hu H 1974 *Can. Metall. Q.* **13** 275
Kapadia C M and Leipold M H 1974 *J. Am. Ceram. Soc.* **57** 41
Kawasaki K 1990 *Physica* A **163** 59
Kawasaki K and Enomoto Y 1988 *Physica* A **150** 462
Kawasaki K, Nagai T and Nakashima K 1989 *Phil. Mag.* B **60** 399
Kermode J P and Weaire D 1990 *Comput. Phys. Commun.* **60** 75
Kraynik A M 1988 *Annu. Rev. Fluid Mech.* **20** 325
Kraynik A M and Hansen M G 1986 *J. Rheol.* **30** 409
Kurtz S K and Carpay F M A 1981 *J. Appl. Phys.* **51** 5725
Lei H 1990 *MSc Thesis* Trinity College, Dublin
Lewis F T 1923 *Proc. Am. Acad. Arts Sci.* **58** 537
Lifschitz I M and Slyozov V V 1959 *Sov. Phys.–JETP* **35** 331
—— 1961 *J. Phys. Chem. Solids* **19** 35
Lindly O 1991 *Nature* **349** 12
Lösche M and Möhwald H 1984 *Rev. Sci. Instrum.* **55** 1968
Marder M 1987 *Phys. Rev.* A **36** 438
Martin J W and Doherty R D 1976 *Stability of Microstructure in Metallic Systems* (Cambridge: Cambridge University Press) p 221
Matzke E B 1945 *Proc. Natl. Acad. Sci. (USA)* **31** 281
—— 1946 *Am. J. Bot.* **33** 58
Matzke E B and Nestler J 1946 *Am. J. Bot.* **33** 130
McDermott M L, Watsky M A, Geroski D H and Edelhauser H F 1990 *Current Eye Res.* **9** 1129
Moore B, Knobler C M, Broseta D and Rondelez F 1986 *J. Chem. Soc., Faraday Trans.* **82** 1753
Nagai T, Kawasaki K and Nakashima K 1988 *J. Phys. Soc. Japan* **57** 2221
Nagai T, Ohta S, Kawasaki K and Okuzono T 1990 *Phase Transitions* **28** 177
Nakashima K, Nagai T and Kawasaki K 1989 *J. Stat. Phys.* **57** 759
Plateau J 1843 *Mem. Acad. R. Belg.* **16** continuing in subsequent issues through 1873
—— 1873 *Statique Experimentale et Theorique des Liquides Soumis aux Seulles Forces Moleculaires* (Paris: Gauthier-Villars)
Smith C S 1952 *Metal Interfaces* (Cleveland, OH: American Society for Metals) p 65
—— 1954 *Sci. Am.* **190** 58
—— 1964a *Rev. Mod. Phys.* **36** 524
—— 1964b *Met. Rev.* **9** 1
Srolovitz D J, Anderson M P, Sahni P S and Grest G S 1984 *Acta Metall.* **32** 793
Stavans J 1990 *Phys. Rev.* A **42** 5049
Stavans J, Dohamy E and Mukamel D 1991 *Europhys. Lett.* **15** 479
Stavans J and Glazier J A 1989 *Phys. Rev. Lett.* **62** 1318
Stine K J, Rauseo S A, Moore B G, Wise J A and Knobler C M 1990 *Phys. Rev.* A **41** 6884
Takasugi T and Izumi O 1985 *Acta Metall.* **33** 49
Thompson C V, Frost H J and Spaepen F 1987 *Acta Metall.* **35** 887
von Neumann J 1952 *Metal Interfaces* (Cleveland, OH: American Society for Metals) p 108
Weaire D and Bolton F 1990 *Phys. Rev. Lett.* **65** 3449
Weaire D, Bolton F, Molho P and Glazier J A 1991 *J. Phys.: Condens. Matter* **3** 2101
Weaire D and Kermode J P 1983a *Phil. Mag.* B **47** L29
—— 1983b *Phil. Mag.* B **48** 245
—— 1984 *Phil. Mag.* B **50** 379
Weaire D and Lei H 1990 *Phil. Mag. Lett.* **62** 47
Weaire D and Rivier N 1984 *Contemp. Phys.* **25** 59
Wejchert J, Weaire D and Kermode J P 1986 *Phil. Mag.* B **53** 15
Wolfe R and North J C 1974 *Appl. Phys. Lett.* **25** 122